

The ^{57}Fe Synchrotron Mössbauer Source at the ESRF

Vasily Potapkin,^{a,b*} Aleksandr I. Chumakov,^{a,c} Gennadii V. Smirnov,^c
Jean-Philippe Celse,^a Rudolf Rüffer,^a Catherine McCammon^b and
Leonid Dubrovinsky^b

^aEuropean Synchrotron Radiation Facility, BP 220, F-38043 Grenoble, France, ^bBayerisches Geoinstitut, Universität Bayreuth, D-95440 Bayreuth, Germany, and ^cNational Research Centre 'Kurchatov Institute', 123182 Moscow, Russian Federation. E-mail: potapkin@esrf.fr

The design of a ^{57}Fe Synchrotron Mössbauer Source (SMS) for energy-domain Mössbauer spectroscopy using synchrotron radiation at the Nuclear Resonance beamline (ID18) at the European Synchrotron Radiation Facility is described. The SMS is based on a nuclear resonant monochromator employing pure nuclear reflections of an iron borate ($^{57}\text{FeBO}_3$) crystal. The source provides ^{57}Fe resonant radiation at 14.4 keV within a bandwidth of 15 neV which is tunable in energy over a range of about ± 0.6 μeV . In contrast to radioactive sources, the beam of γ -radiation emitted by the SMS is almost fully resonant and fully polarized, has high brilliance and can be focused to a $10\ \mu\text{m} \times 5\ \mu\text{m}$ spot size. Applications include, among others, the study of very small samples under extreme conditions, for example at ultrahigh pressure or combined high pressure and high temperature, and thin films under ultrahigh vacuum. The small cross section of the beam and its high intensity allow for rapid collection of Mössbauer data. For example, the measuring time of a spectrum for a sample in a diamond anvil cell at ~ 100 GPa is around 10 min, whereas such an experiment with a radioactive point source would take more than one week and the data quality would be considerably less. The SMS is optimized for highest intensity and best energy resolution, which is achieved by collimation of the incident synchrotron radiation beam and thus illumination of the high-quality iron borate crystal within a narrow angular range around an optimal position of the rocking curve. The SMS is permanently located in an optics hutch and is operational immediately after moving it into the incident beam. The SMS is an in-line monochromator, *i.e.* the beam emitted by the SMS is directed almost exactly along the incident synchrotron radiation beam. Thus, the SMS can be easily utilized with all existing sample environments in the experimental hutches of the beamline. Owing to a very strong suppression of electronic scattering for pure nuclear reflections ($\sim 10^{-9}$), SMS operation does not require any gating of the prompt electronic scattering. Thus, the SMS can be utilized in any mode of storage ring operation.

1. Introduction

Conventional Mössbauer spectroscopy has been a valuable tool for decades in studying the magnetic and electronic properties of various materials. However, the technique is not well suited to the study of samples with diameters of less than $\sim 100\ \mu\text{m}$. Focusing radiation from radioactive sources is extremely difficult (Yoshida *et al.*, 2009) and results in a low count rate and a reduction of spectral quality owing to an increase of the background. This leads to longer measuring

times in order to obtain reasonable quality spectra, and even precludes some studies under extreme conditions, for example the investigation of minerals relevant to the deep Earth at pressures of more than 100 GPa. Thus, the absence of focusing possibilities retards progress in research fields where micro-metre-scale samples are involved, for example high-pressure geophysics and geochemistry.

The time-domain analog of traditional Mössbauer spectroscopy is realised *via* time-resolved nuclear forward scattering (NFS) of synchrotron radiation. Synchrotron radiation

has very high brilliance and allows for extreme focusing; hence NFS is an excellent tool for studying micrometre-sized samples. However, NFS is not well suited to studying highly complex phases which contain iron in different spin states, valence states and crystallographic sites. The time spectrum of NFS results from an interference of waves coherently scattered by all iron atoms in the sample; therefore it also contains the cross-terms of the scattering amplitudes of iron atoms in different states. Thus, in order to derive the hyperfine parameters for one iron state or site, one needs to fit the hyperfine parameters of all states. In contrast, absorption, by nature, is an incoherent process, and results in an energy spectrum, which is a linear superposition of constituent components. In most cases this enables the fitting of each iron site or state independently from all others; hence energy-domain Mössbauer spectroscopy is more suitable for studying highly complex phases. Thus for studies of micrometre-scale absorbers with complex Mössbauer spectra, the optimum approach would be to employ high-resolution energy-domain Mössbauer spectroscopy in combination with high brilliance and extreme focusing of synchrotron radiation. In short, what is needed is a synchrotron-based source of Mössbauer radiation.

Such a source can be designed for ^{57}Fe using the properties of pure nuclear reflections of an iron borate crystal. For reflections of this type, electronic diffraction is forbidden, but nuclear diffraction is allowed because of a specific polarization factor of nuclear resonant scattering in the presence of hyperfine interactions (Smirnov *et al.*, 1969). Owing to magnetic hyperfine splitting of the ^{57}Fe nuclear levels in the ground and the first excited states, the energy spectrum of the reflected radiation consists of several lines. Under these conditions the nuclear array in a crystal behaves as a multiline radiator. This is, of course, an inconvenient property for performing spectroscopic measurements. However, when the iron borate crystal is heated close to its Néel temperature of 348.35 K, the energy spectrum of the reflected radiation collapses to a single line (Smirnov *et al.*, 1986). Under these conditions a particular case of hyperfine interaction is realised where magnetic dipole and electric quadrupole hyperfine interactions are strongly mixed (Smirnov, 2000). The combined multipath quantum interference in space, energy and spin domains results in the formation of a pseudo-single-line resonance structure in iron borate (Smirnov *et al.*, 2011), which provides the basis for the creation of a single-line Synchrotron Mössbauer Source (SMS). The spectrum of the emitted radiation has an energy bandwidth close to the natural line width of the Mössbauer resonance. The possibility to develop such a source was demonstrated at the European Synchrotron Radiation Facility (ESRF) in 1997 (Smirnov *et al.*, 1997). Later, the same approach was successfully implemented at SPring-8 (Mitsui *et al.*, 2007a,b,c, 2009).

For energy-domain Mössbauer spectroscopy one needs to scan the energy by changing the relative velocity of the source and the sample using the Doppler effect. In SMS experiments several methods exist to achieve the Doppler effect. The simplest is to move the sample (Smirnov *et al.*, 1997; Mitsui *et*

al., 2007a,b); however, this approach is not convenient for most experiments where generally a complicated and/or a heavy sample environment is used. Another possibility is to use an additional silicon crystal before the sample and to achieve the Doppler shift through motion of this crystal (Mitsui *et al.*, 2007c). This removes the limitation on the sample environment; however, the displacement of the Si crystal results in a periodic displacement of the reflected beam and, thus, compromises the focusing. Finally, the Doppler shift can be achieved by moving the iron borate crystal in the plane of the crystal surface (Mitsui *et al.*, 2009). This allows for both preserving the extreme focusing and employing complicated and/or heavy sample environments.

Pure nuclear reflection of the iron borate crystal can be used as either the source of radiation for Mössbauer spectroscopy (Smirnov *et al.*, 1997; Mitsui *et al.*, 2007a,c) or as the analyzer of radiation passed through the sample (Mitsui *et al.*, 2007b, 2009). The first approach allows for an efficient focusing of the beam on the sample in both horizontal and vertical directions. In contrast, when the crystal is used as an analyzer, the focusing of the beam in one direction is usually omitted, because the iron borate crystal would not accept the highly divergent (focused) beam (Mitsui *et al.*, 2007b, 2009), which would lead to a larger spot size and lower count rate. On the other hand, the second approach allows for an easy change in the experiment from collecting SMS spectra to nuclear inelastic scattering (NIS) or NFS, because the change of the technique does not require re-adjustment of the focusing optics and the sample. In contrast, using the iron borate crystal as the source normally implies that both the focusing optics and the sample have to be re-aligned (Smirnov *et al.*, 1997; Mitsui *et al.*, 2007a,c).

In this paper we describe the SMS constructed at the Nuclear Resonance beamline (ID18) (Rüffer & Chumakov, 1996) of the ESRF. The source is optimized for highest intensity and best energy resolution. These qualities are achieved firstly by making use of a highly perfect crystal, secondly by providing a high stabilization of its angular position, and thirdly by using an incident beam of small angular divergence (the necessity of these conditions discussed in §2.5). Furthermore, the source is optimized both for extreme focusing and for practical convenience: the iron borate crystal is used as a source, which allows for focusing in both directions. Moreover, the SMS is built as an in-line monochromator: the beam emitted by the source is directed almost exactly along the incident synchrotron beam; therefore the focusing optics and the sample position require only a small (if any) re-adjustment when moving from SMS to NIS, NFS or diffraction techniques. This also allows for easy use of any possible sample environment in the downstream experimental hutches (such as a high-pressure high-temperature set-up, ultra-high-vacuum system, cryomagnet, *etc.*). The source is designed to be permanently ready for operation, without complicated and time-consuming preparation. For this purpose it is located in the optics hutch and is operational immediately after moving it to the incident beam position.

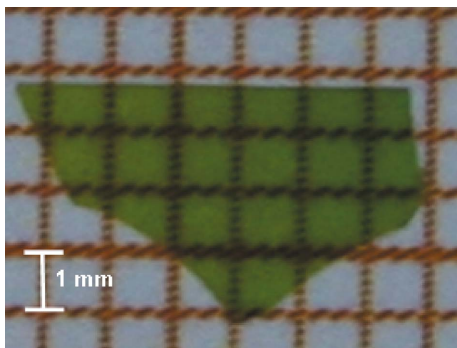


Figure 1
High-quality single-crystal platelet of $^{57}\text{FeBO}_3$ on millimetre graph paper.

2. Synchrotron Mössbauer Source

2.1. Iron borate crystal

The key element of the source that provides neV resolution is the iron borate $^{57}\text{FeBO}_3$ single crystal enriched in the ^{57}Fe isotope up to 95%, grown by Kotrbová *et al.* (1985). One of the high-quality crystals is shown in Fig. 1. The size of the crystalline platelet is $\sim 5\text{ mm} \times 3\text{ mm}$ and the thickness is $\sim 35\text{ }\mu\text{m}$. Iron borate is a canted antiferromagnet with a Néel temperature of 348.35 K. In this crystal all (*NNN*) reflections with odd *N* [*i.e.* (111), (333), *etc.*] are forbidden for electronic diffraction, while on the other hand they are allowed for nuclear diffraction. These are the so-called pure nuclear reflections. The planes (*NNN*) are parallel to the platelet surface. Therefore, the considered reflections are the symmetric ones.

2.2. Pure nuclear reflections

The electronically forbidden but nuclear allowed reflections are employed to extract the nuclear scattering signal. This is possible because of the large difference in the polarization dependence of the electronic and nuclear scattering amplitudes and the antiferromagnetic ordering of iron atom spins in the FeBO_3 crystal. The sensitivity of nuclear scattering to the orientation of the magnetic field introduces an additional phase π between waves scattered by two nuclei in the crystallographic unit cell and thus it converts the destructive interference between the waves to a constructive one (Smirnov *et al.*, 1969). In this way the structural restriction forbidding reflections from the nuclear lattice is removed.

In the presence of hyperfine splitting of the nuclear levels, however, the crystal functions as a multiline nuclear radiator. Such a source is obviously not convenient for spectroscopic studies. Yet a special case of combined magnetic dipole and electric quadrupole interactions can be realised in iron borate close to its Néel temperature in the presence of a weak external magnetic field, where a single-line spectrum of emitted radiation can be obtained (Smirnov *et al.*, 1986, 1997; Smirnov, 2000; Mitsui *et al.*, 2009). The energy width of the emitted line is close to the natural width of the Mössbauer resonance and is very sensitive to the temperature and

magnetic field applied across the crystal (Smirnov *et al.*, 2011). Therefore, in order to avoid inhomogeneous broadening of the source (for an optimal operation of the SMS), a high degree of homogeneity of both temperature and external magnetic field over the iron borate crystal is required.

2.3. Furnace

The design of the furnace is optimized for homogeneous temperature distribution. Fig. 2(a) shows a general view of the furnace with the attached magnet holder. Heating is provided by two thermo-foils, which are attached from the inside to the bottom part and to the upper cover (Fig. 2b). In order to decrease air convection, the furnace has a small and enclosed heating volume with Kapton foils to cover the windows. The temperature gradient was estimated by comparison of the time spectra of radiation reflected from different parts of the crystal. The time spectra were observed to be rather sensitive to temperature, while the estimation did not reveal any temperature gradient within an accuracy of 0.03 K over 0.2 mm. The total weight of the furnace with attached magnets is 44 g.

The temperature is measured by a Pt100 temperature sensor which is located inside the crystal holder, close to the bottom heating foil. The stability of the temperature control is about 0.01 K.

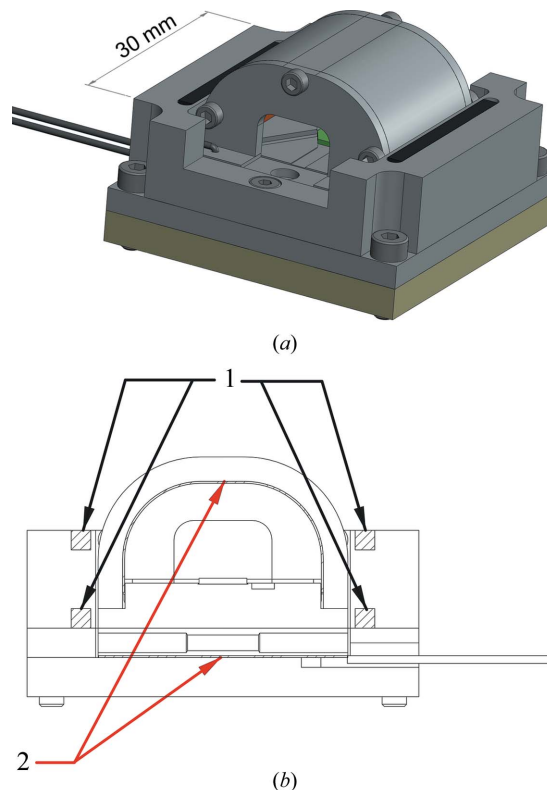


Figure 2
Furnace for the iron borate crystal: (a) a general view of the furnace; (b) a cross section of the furnace: 1, array of four permanent magnets; 2, heating elements located in both the crystal support and in the furnace cover.

2.4. Magnetic field

An external magnetic field is applied to the iron borate crystal for two reasons: firstly, an external magnetic field is required in order to align the magnetic hyperfine field in the plane of the crystal and the scattering plane. This orientation corresponds to a maximum reflection coefficient. Iron borate is a canted antiferromagnet, and the external field needs to be applied perpendicular to the scattering plane in order to correctly orient the magnetic hyperfine field. Secondly, the application of an external magnetic field flattens the temperature dependence of the magnetization near the Néel point (otherwise this dependence is too steep) and extends the magnetization to slightly above the Néel point. This enables easier control of the magnetic hyperfine field, and, therefore, of the spectrum of the reflected radiation.

The external magnetic field should be close to homogeneous over the iron borate crystal, because a variation of the external magnetic field causes a change in the shape of the temperature dependence of magnetization. Correspondingly, a variation of the external magnetic field also leads to a change in the internal magnetic field of the crystal. Using results presented by Zelepukhin *et al.* (1985) we calculated that a variation of the external field of 5 Oe leads to the same variation in the internal field as resulting from a change in crystal temperature of 0.015 K. Our results show that the minimum step over temperature which leads to variations in energy and time distributions of SMS radiation (*i.e.* to detectable change of the internal magnetic field) is 0.03 K. Therefore, the accuracy of internal magnetic field control of the temperature scale should be at least ± 0.015 K or of the magnetic field scale ± 5 Oe.

The external magnetic field on the iron borate crystal is provided by four permanent $\text{Nd}_2\text{Fe}_{14}\text{B}$ magnets located outside of the furnace (Fig. 2*b*). Calculations show that the array of four magnets provides a significantly more homogeneous field than the one resulting from only two magnets. A schematic view of the magnet arrangement is shown in Fig. 3(*a*), where the iron borate crystal is located in the centre of symmetry of the magnet system. The average value of the external magnetic field over the crystal is 110 Oe, with a variation over the crystal of ± 4 Oe or $\pm 3\%$ (Fig. 3*b*), which is within the requirements of the field homogeneity (± 5 Oe).

2.5. Angular position

The intensity of a pure nuclear reflection is a non-trivial function of both the energy of the incident radiation and the angle of incidence. Because the energy bandwidth of the incident synchrotron radiation greatly exceeds the energies of the hyperfine interaction, the reflected beam contains all components of the hyperfine structure. Thus, the rocking curve measured in the experiment, *i.e.* the dependence of the intensity of the reflected beam on the angle of incidence, is the energy-integrated function. Similar to characteristics of hyperfine splitting, the shape and width of the rocking curve of the iron borate crystal significantly depends on temperature. When the crystal is heated from room temperature to its Néel

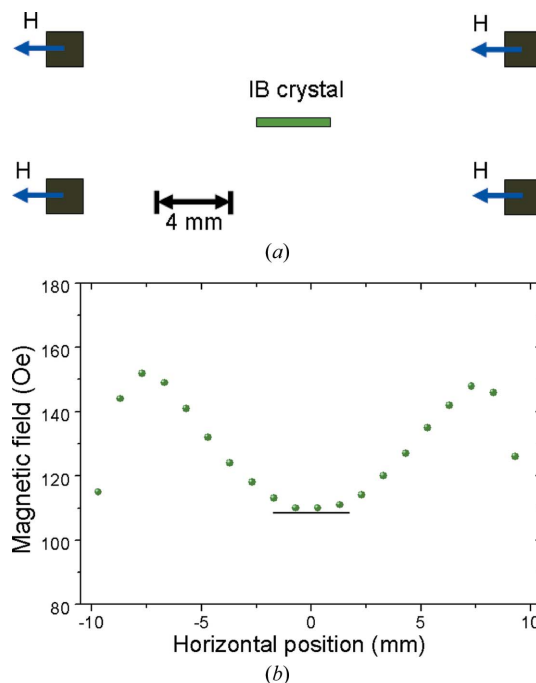
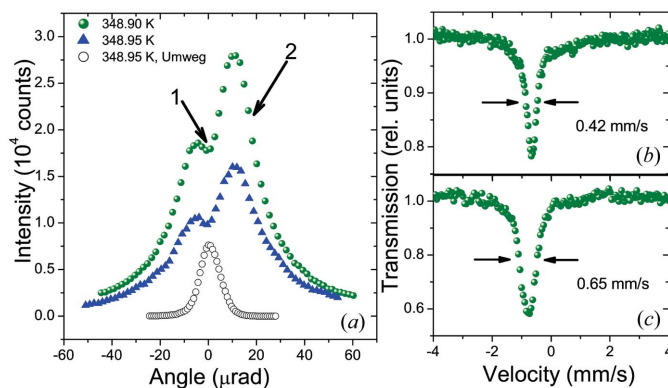


Figure 3
(*a*) Geometric arrangement of the permanent magnets. (*b*) The dependence of the magnetic field (H) on the horizontal position along the crystal surface in the direction perpendicular to the incident beam. The horizontal bar in both pictures denotes the location of the iron borate crystal.

transition, the angular width of the rocking curve increases by more than one order of magnitude. As found by Smirnov *et al.* (2011), the rocking curve strongly broadens near the Néel temperature and transforms to a double-hump structure with a central dip between the peaks. The angular position of the dip corresponds to the exact Bragg angle. Near the Néel temperature the angular width ceases to increase and approaches a finite maximum value (Smirnov *et al.*, 2011).

Examples of the rocking curve measured close to the Néel temperature are shown in Fig. 4(*a*). The large (~ 40 μrad) angular width of the nuclear reflection is undoubtedly related to the transformation of the Mössbauer diffraction spectrum in the vicinity of the Néel temperature (Smirnov *et al.*, 2011). For instance, it cannot be attributed to a possible curvature of the crystal. This has been verified by measurements at the same temperature of the rocking curve for electronic Umweg reflections (see below). The intrinsic angular width of Umweg reflections can be very narrow; therefore the width of an Umweg reflection measured in the experiment is essentially a convolution of the angular divergence of the incident beam and the effective crystal curvature. Fig. 4(*a*) shows that this value (~ 10 μrad) is much less than the width of the rocking curve of nuclear reflection.

The energy spectrum of radiation emitted by the excited nuclear array strongly depends on the angular position of the crystal relative to the incident beam [see Fig. 7 of Smirnov *et al.* (2011)]. In terms of Mössbauer spectroscopy, this spectrum represents the instrumental function of the SMS. At the centre of the dip between the peaks of the rocking curve (*i.e.* at the


Figure 4

(a) Rocking curves of the pure nuclear (333) reflection (in absolute vertical scale) and of the electronic Umweg reflection (arbitrary vertical scale) of the $^{57}\text{FeBO}_3$ crystal for temperatures in the vicinity of the Néel point. The arrows show the angular positions where the Mössbauer absorption spectra were measured. (b) and (c) Mössbauer absorption spectra of the single-line absorber measured at angular positions 1 and 2, respectively, at an iron borate crystal temperature of 348.90 K.

exact Bragg position), the spectrum of the reflected radiation consists predominantly of a single line having a width of about the natural resonance line width Γ_0 (Smirnov *et al.*, 2011). Thus, this angular position provides the optimal instrumental function of the source. When the crystal is detuned from the exact Bragg angle, the tails of the single line appear at the lower and/or the upper part of the energy spectrum (Smirnov *et al.*, 2011). In this case the instrumental function, besides the single-line component, contains additional satellite peak(s), which can lead to the appearance of artefacts in the measured Mössbauer spectra.

In the experiment, a finite divergence of the incident beam and/or a certain bending of the crystal lattice may lead to a noticeable weakening of the dip in between the peaks of the rocking curve and hence can cause some angular averaging of the instrumental function over incidence angles with a corresponding deterioration of its quality. Thus, in order to preserve a good quality of the instrumental function and a high intensity, one needs to have a high-quality iron borate single crystal, a small divergence of the incident beam, and a sufficiently accurate rotational stage for precise and stable angular positioning of the crystal.

In approaching the Néel temperature, the angular width of the rocking curve increases. Accordingly, the dip between the two peaks of the rocking curve where the single-line instrumental function can be obtained becomes more distinct and broad, making it easier to maintain the crystal at the optimal angular position. Furthermore, the broadening of the rocking curve is accompanied by a narrowing of the energy spectrum of radiation reflected by the crystal at the exact Bragg angle (Smirnov *et al.*, 2011). Thus, increasing temperature improves the instrumental function of the SMS. However, this improvement is accompanied by a strong decrease of the intensity of the reflected radiation; therefore a reasonable compromise between the quality of the instrumental function and the count rate has to be found. Under otherwise equivalent conditions, a good quality of the crystal and a proper

collimation of the incident beam should allow one to achieve this compromise at higher intensity.

Fig. 4(a) shows the rocking curves of the (333) reflection for two different temperatures in the vicinity of the Néel point. The first rocking curve (green circles) is obtained at a temperature of 348.90 K where an optimal compromise between the energy width of the instrumental function and the intensity of the reflected beam is achieved. The second rocking curve shown in Fig. 4(a) (blue triangles) is measured at a temperature 0.05 K above the previous one. This small change of temperature increases the width of the rocking curve from 33 μrad to 37 μrad , which slightly relaxes the requirements for collimation of the beam, quality of the crystal and angular stability. However, this lowering of the tolerance to angular distortions is accompanied by $\sim 40\%$ loss of intensity. Thus, even small improvements of the beam collimation and crystal quality could provide a tremendous gain in the efficiency of the SMS.

The instrumental functions of the SMS were evaluated using a single-line $\text{K}_2\text{Mg}^{57}\text{Fe}(\text{CN})_6$ absorber with an area density of the resonant ^{57}Fe isotope of 0.50 mg cm^{-2} and a line width of $2.1 \Gamma_0$ ($\Gamma_0 = 0.097 \text{ mm s}^{-1}$). For analysis of the source radiation [Figs. 4(b) and 4(c)], the source was moved to modulate the energy of γ -radiation. Fig. 4(b) shows the absorption spectrum measured when the iron borate was set to the angular position at the centre of the dip on the rocking curve (Fig. 4a). The obtained line width of $4.3 \Gamma_0$ testifies that the line width of the instrumental function at the optimal angular position is about $2.2 \Gamma_0$. Here and below the isomer shifts are shown as measured. In particular, the isomer shift is given relative to the SMS. The isomer shift of α -Fe relative to the SMS is $-0.786(3) \text{ mm s}^{-1}$. It is important to note that in order to obtain the energy distribution of the radiation reflected by the iron borate crystal [see Fig. 7 in Smirnov *et al.* (2011)] one needs to invert the velocity scales in the spectra presented in Fig. 4.

At the angular positions of both peaks of the rocking curve the instrumental function acquires undesirable satellite peaks. The same effect happens when the iron borate crystal is not of sufficient quality: the double-peak structure is washed out and the instrumental function measured at the exact Bragg angle acquires satellite peaks owing to the effective angular averaging. Under these conditions a single-line absorption spectrum can be obtained at the 'backup' angular position at the high-angle slope of the rocking curve (Fig. 4a). However, the energy width of the instrumental function at the backup position is larger: the measured line width of $6.7 \Gamma_0$ (Fig. 4c) shows that the line width of the instrumental function is about $4.6 \Gamma_0$.

2.6. Umweg reflections

Even if a particular reflection is forbidden for electronic diffraction, the X-ray beam may find a way for multiple scattering in the crystal lattice. The X-rays may experience diffraction on two or more sets of crystalline planes so that the beam is reflected in the same direction as if the reflection

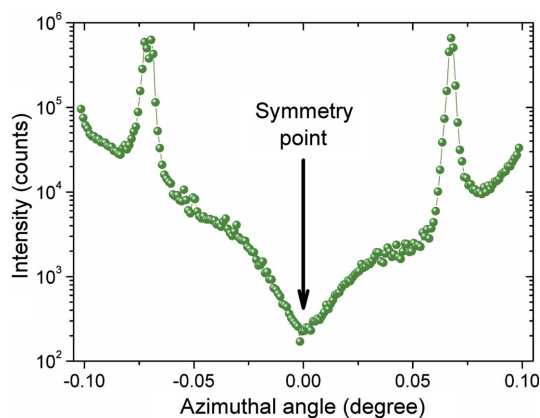


Figure 5 Azimuthal dependence of Umweg reflections for the pure nuclear (111) reflection of the iron borate crystal in the vicinity of the azimuthal position along the $[10\bar{1}]$ crystallographic direction. The data were taken at 353.15 K.

would be allowed. Such ‘bypass’ reflections are called Umweg reflections (Renninger, 1937). These reflections are characterized by a broad energy bandwidth typical for electronic diffraction. The Umweg reflections may add intense non-resonant radiation to the reflected beam, thus creating a strong non-resonant background in the Mössbauer spectrum. In order to avoid this background, one needs to escape Bragg conditions for one or more sets of planes involved in Umweg reflections while preserving the Bragg condition for pure nuclear reflection. This can be achieved by rotating the iron borate crystal around the axis of the scattering vector, *i.e.* by scanning the azimuthal angle of the crystal. For the crystal of iron borate, the azimuthal dependence of the (NNN) Umweg reflections has sixfold symmetry and 12 symmetry points, which correspond to the $[11\bar{2}]$ and $[10\bar{1}]$ crystallographic directions. Fig. 5 shows the azimuthal dependence of the Umweg reflections in the vicinity of the $[10\bar{1}]$ direction for the (111) pure nuclear reflection. For this measurement the crystal was heated well above its Néel temperature, where nuclear scattering was completely suppressed and the monitored intensity originated only from electronic scattering of the Umweg reflections. Near the $[10\bar{1}]$ symmetry point the tails of the neighbouring Umweg reflections fortunately cancel each other out (Fig. 5). Thus, at this particular azimuthal position the non-resonant background in the absorption Mössbauer spectra taken with the SMS is suppressed almost completely.

The intensity of prompt electronic scattering in Umweg reflections is much higher than the intensity of resonant scattering of pure nuclear reflections and may be used to advantage. In particular, with Umweg reflections it is much easier to align the sample inside the diamond anvil cell (DAC) to the beam and to adjust focusing optics.

2.7. Energy modulation

The furnace with the iron borate crystal is mounted on a standard Mössbauer transducer, which moves the crystal in the plane parallel to the crystal surface. There are several approaches to understand how the energy modulation of the

reflected beam occurs: considering the SMS as a monochromator, one notes that the motion of the crystal along its surface does not change the energy of the X rays. Indeed, the utilized pure nuclear (NNN) reflections are symmetric. Therefore, the incoming and outgoing beams form equal angles with the plane of motion, and the Doppler shift in frequency of the incoming radiation is compensated by exactly the opposite Doppler shift of outgoing radiation. Thus the frequency of the incoming radiation is transmitted to the same frequency of the outgoing radiation. In the case of electronic scattering the atomic scattering amplitude is constant within the range of the Doppler shift. However, nuclei can only be excited by the frequency equal to their own resonant frequency. By moving nuclei with different velocities one can effectively change the resonant frequency of the nuclei. The bandwidth of the resonant energy is much less than the range of the Doppler shifts. On the other hand, the bandwidth of incoming radiation is larger than the Doppler shift range. Therefore, nuclei being moved with different velocities effectively select from the incoming beam the radiation components with different frequencies. In this way the energy modulation of the reflected radiation is achieved. Alternatively, one may consider the SMS as a coherent radiator of nuclear γ -rays. The ^{57}Fe nuclei of the iron borate crystal are excited by the white spectrum of incident radiation for any velocity of the moving crystal. After excitation, the nuclei emit nuclear γ -radiation. The energy of this radiation is equal to the energy of the nuclear resonant transition. Similar to a conventional radioactive source, the translational motion of the iron borate crystal causes a Doppler shift and leads to the energy modulation of the emitted radiation.

In contrast to other approaches to obtain the Doppler shift (Mitsui *et al.*, 2007c), moving the iron borate crystal along the plane of the crystal surface has an important advantage: this motion does not cause a spatial displacement of the reflected beam. Therefore, the energy modulation does not compromise focusing and does not shift the beam relative to the sample (Mitsui *et al.*, 2007d).

From the point of view of oscillatory dynamics, ideally the furnace should be located at the centre of inertia of the moving frame of the transducer. However, this requirement is difficult to combine with the diffraction geometry. To allow for diffraction, the furnace is attached to the moving frame above the transducer (Fig. 6). Under such conditions the frame is obviously not balanced, *i.e.* its centre of mass is shifted upwards from the axis of the transducer. This shift leads to the appearance of an inertial force torque. Under these conditions the translation movement of the frame would be accompanied by rocking motions, which would result in a variation of the angle between the incident radiation and the crystal during the crystal motion. This would cause (i) broadening of the instrumental function and (ii) oscillations of the intensity of the reflected beam. Obviously, the quality of Mössbauer spectra with such a source would be significantly lower; firstly, because of diminished energy resolution and, secondly, because the base line (*i.e.* the Mössbauer spectrum collected without sample) would no longer be flat.

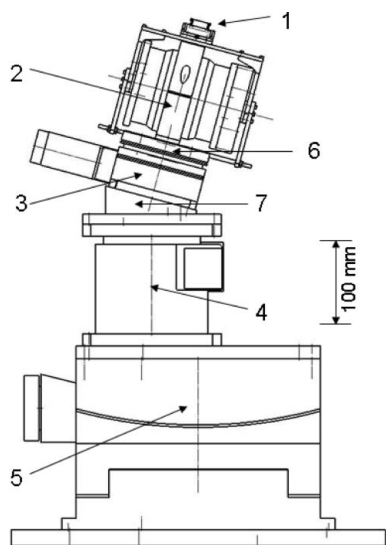


Figure 6
Mechanics of the synchrotron Mössbauer source: (1) furnace; (2) transducer; (3) one-circle goniometer for azimuthal rotation; (4) vertical translation stage; (5) two-circle segment for Bragg and tilt rotations; (6) counterweight of the frame; (7) wedge.

In order to avoid these drawbacks, the frame is balanced by a counterweight which is mounted on the bottom side of the frame below the transducer. The distances from the axis of the transducer to the counterweight and to the furnace are equal.

For adjustment of the mass of the counterweight, the furnace is exchanged by a silicon crystal with a mass equal to the mass of the furnace. The angular stability of the frame during its translational motion is evaluated by monitoring the intensity of the beam reflected by the silicon crystal as a function of the velocity of the frame. With a properly adjusted mass of the counterweight, the measured base line is straight. In order to reach the highest sensitivity of the adjustment, the base line is measured at the half-maximum position of the rocking curve of the silicon crystal.

After adjustment of the counterweight, the estimated residual variation of the angular position of the frame is about $1 \mu\text{rad}$. This is ten times smaller than the width of the angular range near the exact Bragg angle of the pure nuclear (333) reflection of the iron borate crystal where the single-line spectrum of the instrumental function can be achieved.

2.8. Mechanics of the SMS

In order to operate the SMS, the following rotations and translations of the iron borate crystal are required: firstly, one needs a very accurate rotation stage to adjust the Bragg angle of the crystal. Secondly, in order to avoid Umweg reflections, an azimuthal rotation is needed. Finally, the tilt rotation of the crystal is needed to keep the reflected beam in the vertical plane. All these rotational stages should be precise and stable. In addition, two translations (a horizontal and a vertical one) are needed to adjust the crystal position relative to the incident synchrotron radiation beam.

Fig. 6 shows a schematic view of the mechanics of the SMS. The bottom part is a large two-circle segment (Huber 2-circle segments 5203.80), and the iron borate crystal is located at the centre of rotation of this segment. One circle is utilized for Bragg angle adjustments and is equipped with a 20:1 gear box. The accuracy of angular positioning of this rotation stage is about $0.5 \mu\text{rad}$. The other circle is utilized for tilt angle adjustments; the accuracy of angular positioning of this stage is about $2 \mu\text{rad}$. The vertical translation stage (Huber z-stage 5103.A20-90) is mounted on the two-circle segment; the accuracy of linear positioning provided by this stage is better than $5 \mu\text{m}$. On the vertical translation stage a wedge is mounted which supports the stage of azimuthal rotation. The wedge angle is equal to the Bragg angle of the chosen pure nuclear reflection of the iron borate crystal. The one-circle goniometer (Huber 1-circle goniometer 409) is used for azimuthal rotation and is equipped with a 10:1 gear box. The accuracy of angular positioning provided by this rotation stage is about $5 \mu\text{rad}$. The Mössbauer transducer (Wissel MVT-1000) equipped with the frame and the furnace is mounted on the azimuthal stage. The entire mechanics are mounted on a horizontal translation stage which is used to adjust the horizontal position of the crystal relative to the beam and to move the entire set-up in and out of the beam. The accuracy of linear positioning provided by this stage is about $5 \mu\text{m}$.

3. Optical scheme

3.1. In-line set-up

Apart from the iron borate crystal, the optical scheme of the SMS includes two additional optical elements. The first optical element is an additional monochromator. The beam after the high-heat-load monochromator is so intense that it may produce a temperature gradient over the surface of the iron borate crystal. In order to avoid the temperature gradient, an additional monochromator is needed whose purpose is to decrease the energy bandwidth of the beam incident on the iron borate crystal and thus to decrease the heat load. For this purpose the bandwidth can be chosen to be only moderately (not extremely) small. Under these conditions the additional monochromator can be relatively easily optimized for an essentially high throughput. Therefore, the inclusion of the additional monochromator essentially does not decrease the intensity of the beam provided by the source. The second additional optical element is a deflector. The deflector is needed in order to make the SMS an in-line monochromator. The deflector rotates the beam incident on the iron borate crystal in the vertical plane so that the beam emitted by the crystal is directed almost horizontally, almost exactly along the synchrotron radiation beam from the high-heat-load monochromator.

The choice of the additional monochromator and deflector depends on the utilized pure nuclear reflection. In this paper we describe the in-line optical schemes for the (111) and (333) pure nuclear reflections of the iron borate crystal.

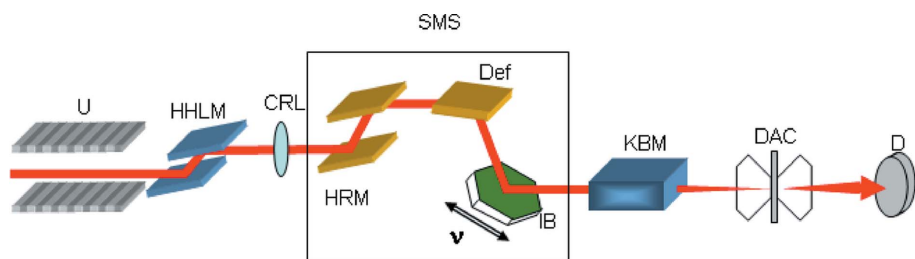


Figure 7
Optical scheme for a high-pressure experiment with the DAC using the Synchrotron Mössbauer Source based on the (333) pure nuclear reflection. U, undulator; HHLM, high-heat-load monochromator; CRL, compound refractive lens; SMS, the Synchrotron Mössbauer Source; HRM, high-resolution monochromator; Def, Si (311) deflector; IB, iron borate crystal inside the furnace with the four magnets and mounted on the Mössbauer transducer; KBM, Kirkpatrick–Baez mirrors; DAC, diamond anvil cell; D, avalanche photodiode detector.

3.1.1. (333) reflection. The pure nuclear (333) reflection of iron borate is convenient for the deflector reflection (311) of silicon. For 14.4 keV radiation the Bragg angle of the silicon (311) reflection is 15.23° and almost matches that of the iron borate (333) reflection (15.49°). Thus, the angle between the beam from the SMS and the horizontal plane is only 0.52° . This enables the beam to reach all downstream experimental hutches and to use all sample environments available at the beamline. This deflector can be easily combined with any additional in-line monochromator. This is a significant advantage of the SMS based on the (333) pure nuclear reflection of iron borate. In this work we use an in-line high-resolution monochromator with a bandwidth of ~ 15 meV. It is a double-crystal monochromator with two asymmetric (975) reflections of silicon crystals.

Fig. 7 shows a typical optical scheme for a high-pressure experiment with a DAC using SMS based on the (333) pure nuclear reflection. The undulator (U) is the source of the synchrotron radiation beam. The high-heat-load monochromator (HHLM) decreases the energy bandwidth of the beam to ~ 2 eV, and the compound refractive lens (CRL) is used to decrease the divergence of the beam incident to the SMS. The high-resolution monochromator (HRM) decreases the energy bandwidth of the beam further to ~ 15 meV. The deflector (Def) directs the beam to the iron borate crystal (IB) where the final monochromatization within ~ 10 neV occurs. The beam from the SMS is focused by the Kirkpatrick–Baez mirrors (KBM) on the sample located in the DAC. The γ -radiation transmitted through the sample is monitored by the avalanche photodiode detector (D).

3.1.2. (111) reflection. Another reasonable option for the SMS is the (111) pure nuclear reflection. The angular width of this reflection is three times larger than that of the (333) one. Therefore, the requirements for the angular stability, crystal quality and collimation of the incident beam are more relaxed. As described above, under otherwise equivalent conditions

this helps to achieve a narrower instrumental function and higher intensity. However, the Bragg angle of the (111) reflection is three times smaller than that of the (333) one. Therefore, the area illuminated by the incident beam on the surface of the iron borate crystal is three times larger. Thus, higher-quality iron borate crystals are required. Furthermore, for the (111) reflection of iron borate there is no convenient reflection of silicon for the deflector with a sufficiently close Bragg angle. The deflector for the (111) reflection can be obtained using two reflections:

Si(422) and Si(531). The difference between the Bragg angles of these reflections is 5.111° while the Bragg angle of the iron borate (111) reflection is 5.108° . Thus, the beam reflected by the {Si(422) + Si(531)} deflector and the iron borate (111) reflection deviates from the horizontal plane by an angle of less than $100 \mu\text{rad}$. This makes the SMS based on the (111) pure nuclear reflection an in-line monochromator. This deflector also decreases the energy bandwidth to ~ 100 meV. Thus, it acts both as a deflector and an additional monochromator. The advantage of this set-up is that one may combine the SMS experiment with any other technique such as inelastic scattering or diffraction: the beam after the SMS based on the (111) pure nuclear reflection matches the path of the incident synchrotron radiation beam within an accuracy of $100 \mu\text{rad}$. Thus, one can move the SMS out of the beam and exchange it with any other in-line monochromator without re-adjusting the focusing optics or sample position.

Fig. 8 shows a typical optical scheme for a high-pressure experiment with a DAC using the SMS based on the (111) pure nuclear reflection. The medium-resolution monochromator (MRM) with silicon reflections Si(422) and Si(531) serves as both an additional monochromator and a deflector. All elements before and after the SMS are the same as for the set-up based on the (333) pure nuclear reflection.

Although most of the problems encountered during source development have been solved, there is one unexpected effect

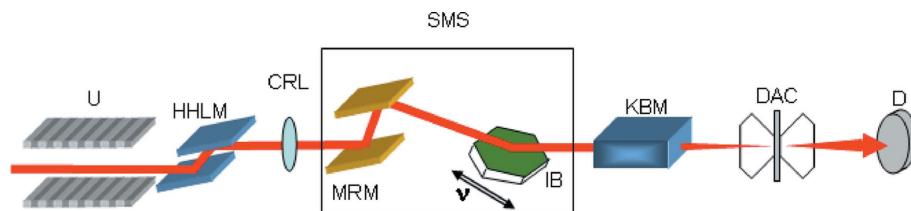


Figure 8
Optical scheme for a high-pressure experiment with a DAC using the Synchrotron Mössbauer Source based on the (111) pure nuclear reflection. U, undulator; HHLM, high-heat-load monochromator; CRL, compound refractive lens; SMS, the Synchrotron Mössbauer Source; MRM, deflector and medium-resolution monochromator with ~ 100 meV bandwidth; IB, iron borate crystal inside the furnace equipped with four magnets and mounted on the Mössbauer transducer; KBM, Kirkpatrick–Baez mirrors; DAC, diamond anvil cell; D, avalanche photodiode detector.

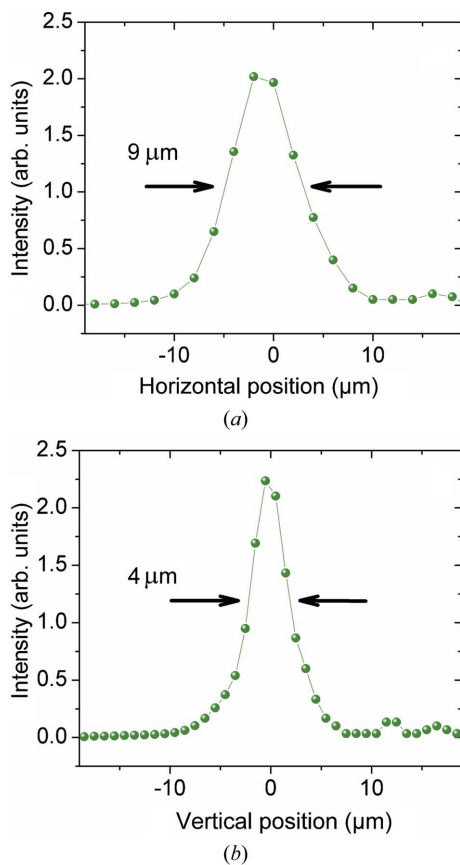


Figure 9 Profiles and sizes of the focal spot in the (a) horizontal and (b) vertical directions. The arrows show the full widths at the half-maximum of the profiles.

that occurs; namely, bending of the initially flat iron borate crystal. The bending appears after about one week of operation and only when the crystal is heated up to its Néel temperature. Although the initial crystal state recovers after a period of relaxation, the bending effect compromises system stability and requires further investigation.

3.2. Focusing

In order to focus the beam after the SMS we use Kirkpatrick–Baez mirrors (KBMs) (Hignette *et al.*, 2001) consisting of graded Ru/B₄C multilayers on a silicon substrate. The active lengths of the mirrors (150 mm) are essentially large in order to accommodate the entire beam. The focal lengths of the mirrors are 950 mm (for vertical focusing) and 630 mm (for horizontal focusing). The KBM system allows one to focus the beam after the SMS to a spot of about 10 μm × 5 μm with 60% throughput. The profiles and the sizes of the focal spot in the horizontal and vertical directions are shown in Fig. 9.

4. Properties of the SMS radiation

4.1. Polarization

Synchrotron radiation is almost fully linearly polarized; therefore the beam emitted by the SMS is also polarized. For

the incident synchrotron radiation the vector of the electric wavefield lies in the horizontal plane. Pure nuclear reflections of the iron borate crystal rotate polarization vectors by 90°. Thus, the beam after the iron borate crystal is also linearly polarized, but the vector of the electric wavefield lies in the vertical plane. The polarization of the beam makes the Mössbauer spectra measured with the SMS extremely sensitive to the direction of the electric field gradient (EFG) and of the magnetic field on nuclei. In studies of single crystals this sensitivity allows for determination of the geometry of the electric field gradient and hyperfine magnetic field. In studies of powder samples the polarization of the SMS radiation leads to a sensitivity to texture in the sample. For isotropic orientation of crystallites (no texture) the spectra measured with the SMS are identical to those measured with non-polarized radiation. However, in the case where texture is present, the SMS spectra will be different. For quadrupole splitting, preferred orientation of the EFG causes area asymmetry in doublet components. For magnetic splitting, preferred orientation of the magnetic field changes the relative intensity of the spectral lines corresponding to nuclear transitions with a change of the nuclear magnetic moment projection $\Delta m = \pm 1$ and those with a change of the magnetic moment projection $\Delta m = 0$.

4.2. Shape of the instrumental function

The energy spectrum of γ -radiation from a radioactive source is a Lorentzian distribution,

$$L(E) \propto \frac{\Gamma_0/2}{(E - E_0)^2 + (\Gamma_0/2)^2}, \quad (1)$$

where Γ_0 is the natural width of nuclear resonance, E is the energy of radiation and E_0 is the resonance energy. In contrast, the energy spectrum of radiation emitted by the SMS is the result of the interference of two spectral lines (each with a Lorentzian distribution) with almost equal resonance energies during the collapse of the magnetic hyperfine structure (Smirnov *et al.*, 2011). Therefore, the energy spectrum of radiation emitted by the SMS to a first approximation can be described by a squared Lorentzian distribution (Smirnov *et al.*, 2011),

$$L^2(E) \propto \left[\frac{\Gamma/2}{(E - E_0)^2 + (\Gamma/2)^2} \right]^2, \quad (2)$$

where Γ is the width of each of the interfering lines. Knowledge of the exact shape of the energy distribution is important for correct fitting of the measured spectra.

4.3. Suppression of electronic scattering

For pure nuclear reflection, electronic scattering is suppressed almost completely to a level of 10^{-9} . Therefore, non-resonant radiation is a negligible part of the source radiation. For example, in the case of a set-up based on the (111) reflection of iron borate, the fraction of non-resonant quanta in the source radiation is ~ 1 –2%. In the case of a set-up based on the (333) reflection, the non-resonant fraction is

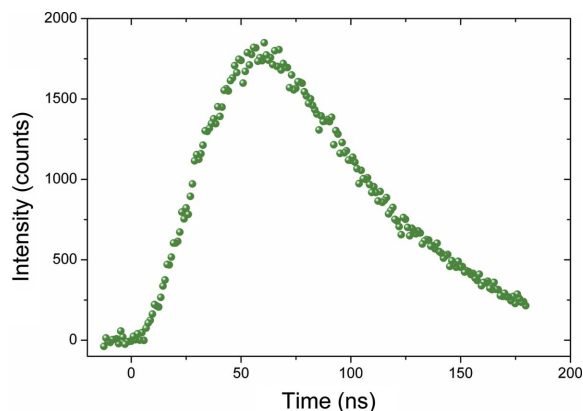


Figure 10
Time distribution of the photons reflected by $^{57}\text{FeBO}_3$ near its Néel temperature. Zero time corresponds to the moment when the synchrotron radiation excites the crystal.

less than $\sim 0.01\%$. This is illustrated by the time distribution of photons reflected by $^{57}\text{FeBO}_3$ shown in Fig. 10. At zero time when synchrotron radiation excites the crystal, there are no prompt quanta of electronic scattering and thus there is no need to gate electronic scattering. SMS spectra are therefore free from artifacts related to gating (Seto *et al.*, 2009) and, moreover, SMS can work in any mode of storage ring operation.

5. Applications

The SMS is well suited to studies of small (micrometre-size) samples which are difficult or impossible to measure with a conventional radioactive source. Therefore, one of the most straightforward applications of the SMS is high-pressure studies with DACs. Using the SMS described in this paper, the spin states of iron in the geologically relevant system of magnesium silicate perovskite ($\text{Mg}_{1-x}\text{Fe}_x(\text{Si}_{1-y}\text{Al}_y)\text{O}_3$) have been studied as a function of composition and pressure in a range relevant to the lower mantle of the Earth (Potapkin *et al.*, 2012).

The data collection time for a Mössbauer spectrum of a sample in a DAC using the SMS is typically three orders of magnitude shorter than using a radioactive source. For example, the measurement of a good quality Mössbauer spectrum of the silicate perovskite sample mentioned above took about 10 min, compared with more than one week using a radioactive point source for the same sample (Potapkin *et al.*, 2012). Moreover, the statistical accuracy of the spectrum measured with a radioactive source is usually lower owing to the strong non-resonant background produced by Compton scattering of the high-energy components of the radioactive source. In contrast, the spectrum measured with the SMS is practically free from the non-resonant background (Compton scattering, recoiled component, *etc.*), allowing for a higher quality of the spectrum.

The short measuring time is even more important for combined high-pressure and high-temperature measurements using laser heating. At present it is difficult for laser heating

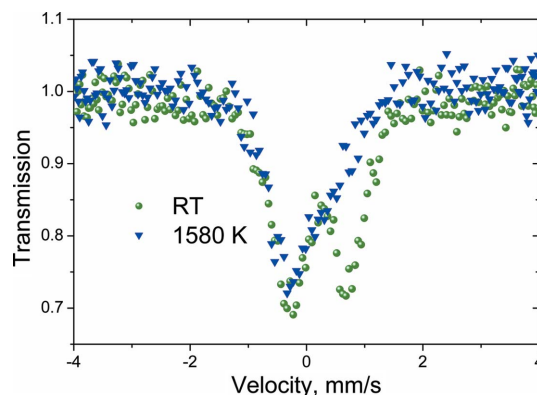


Figure 11
Spectra of $(\text{Mg}_{0.8}\text{Fe}_{0.2})\text{O}$ ferropericlasite at a pressure of 29 GPa at room temperature (green circles) and at 1580 K (blue triangles).

systems to maintain a stable temperature for long periods of time; hence application of a laser heating system for conventional Mössbauer spectroscopy using a radioactive source is extremely challenging. Thus, the SMS is essentially the only tool available for collecting energy-domain Mössbauer spectroscopy at the combined conditions of high temperature and high pressure.

Using the SMS, we have studied several systems at combined conditions of high temperature and high pressure. Fig. 11 shows two examples of measured SMS spectra of $(\text{Mg}_{0.8}\text{Fe}_{0.2})\text{O}$ ferropericlasite. The sample was pressurized in a DAC to 29 GPa and heated using a double-sided laser system to 1580 K, and the measurement time was 10 min per spectrum. The room-temperature spectrum (green circles) shows a Fe^{2+} doublet, while the spectrum collected at 1580 K (blue triangles) shows a strongly asymmetric singlet. The singlet results from the strong decrease of quadrupole splitting in Fe^{2+} ions with increasing temperature, while the asymmetry is likely to be due to a temperature gradient in the sample.

Another application where a small beam size is critical is surface studies, which are usually performed in grazing-incidence geometry (*i.e.* when the incidence angle is close to the critical angle of total external reflection). In order to test the feasibility of such research using the SMS, a ^{57}Fe film on a polished MgO (001) substrate, with a thickness of 8 nm was prepared. The magnetization direction for this film was in the plane of the film and in a direction parallel to the [110] axis of the substrate that had an angle of 45° to the scattering plane. Fig. 12 shows the spectrum of radiation scattered from the film measured at an incident angle of 0.35° , which is slightly larger than the critical angle of total external reflection (0.22°). Under such conditions reflection occurs when the energy of the incident beam is close to the resonant energy. In contrast to Mössbauer spectroscopy in transmission geometry where the spectrum dips below the baseline at resonance energies, in the given reflection geometry the spectrum peaks at resonance energies above an almost negligible baseline (essentially zero); hence the signal-to-noise ratio is extremely high. Thus, a spectrum with a sufficiently high statistical accuracy can be collected over a short time: the spectrum shown in Fig. 12 was measured over only 5 min. In this geometry vertical focusing is

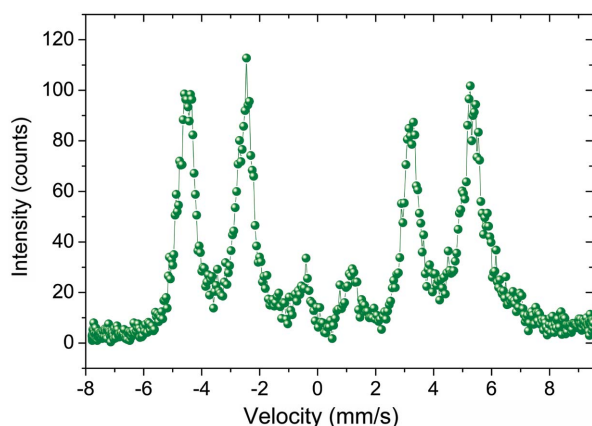


Figure 12

The SMS spectrum of a ^{57}Fe film with a thickness of 8 nm measured in grazing-incidence geometry for a period of 5 min.

needed, otherwise the size of the beam spot is much larger than the sample.

The nuclear resonance beamline ID18 is equipped with a UHV facility (Stankov *et al.*, 2008), which allows for *in situ* investigations of surfaces and thin films. In combination with the UHV facility, the SMS provides the possibility for *in situ* Mössbauer spectroscopy of surfaces and thin films in the energy domain.

6. Conclusions

An SMS for energy-domain Mössbauer experiments has been constructed at the Nuclear Resonance beamline (ID18) of the ESRF. The bandwidth of radiation provided by the SMS is $\sim 3 \Gamma_0$, the intensity is $\sim 2 \times 10^4$ photons s^{-1} and the typical scanning velocity range is about $\pm 12 \text{ mm s}^{-1}$ ($\pm 0.6 \mu\text{eV}$). In contrast to conventional radioactive sources, the SMS gives the possibility to focus the beam to tens of micrometres. It is an in-line monochromator, permanently located in the optics hutch and operational immediately after moving it into the incident beam position. The source can be used with all existing sample environments in the experimental hutches downstream of the beamline.

The implementation of this device opens the possibility for studying systems with complex hyperfine structure under extreme conditions, for example under high pressure. Furthermore, SMS allows for very short collection times of several minutes, which enables use of laser heating. Several high-pressure and high-pressure/high-temperature studies have already been performed. The almost 100% recoilless resonant radiation delivered by the source and its high brightness allow a broad field of SMS applications. Furthermore, SMS can be utilized in any mode of storage ring operation.

The authors would like to thank Ilya Sergeev for help during experiments, for providing computer code for data treatment and for scientific discussions; Marcin Zajac for providing the ^{57}Fe film sample and for help with the surface measurements; Konstantin Glazyrin, Innokenty Kantor, Anastasia Kantor and Ilya Kuppenko for help with the high-pressure/laser-heating studies; Joel Chavanne for modelling of the magnetic system and for providing small permanent magnets; Jean-Pierre Vassalli and Benoit Picut for fabrication of the silicon crystals; and Richard Brand for implementing the version of the computer code *NORMOS* modified to fit the Mössbauer spectra measured with SMS.

References

- Hignette, O., Peffen, J.-C., Alvaro, V., Chinchio, E. & Freund, A. K. (2001). *Proc. SPIE*, **45**, 4501–4510.
- Kotrbová, M., Kadečková, S., Novák, J., Brádlér, J., Smirnov, G. V. & Shvydko, Yu. V. (1985). *J. Cryst. Growth*, **71**, 607–614.
- Mitsui, T., Hirao, N., Ohishi, Y., Masuda, R., Nakamura, Y., Enoki, H., Sakaki, K. & Seto, M. (2009). *J. Synchrotron Rad.* **16**, 723–729.
- Mitsui, T., Seto, M., Hirao, M., Ohishi, Y., Kobayashi, Y., Higashitaniguchi, Y. & Masuda, R. (2007b). *Jpn. J. Appl. Phys.* **46**, L382–L384.
- Mitsui, T., Seto, M., Kikuta, S., Hirao, S., Ohishi, Y., Takei, H., Kobayashi, Y., Kitao, S., Higashitaniguchi, S. & Masuda, R. (2007a). *Jpn. J. Appl. Phys.* **46**, 821–825.
- Mitsui, T., Seto, M. & Masuda, R. (2007d). *Jpn. J. Appl. Phys.* **46**, L930–L932.
- Mitsui, T., Seto, M., Masuda, R., Kiriya, K. & Kobayashi, K. (2007c). *Jpn. J. Appl. Phys.* **46**, L703–L705.
- Potapkin, V., McCammon, C., Glazyrin, K., Kantor, A., Kuppenko, I., Prescher, C., Sinmyo, R., Smirnov, G. V., Popov, S., Chumakov, A. I., Ruffer, R. & Dubrovinsky, L. (2012). *Nat. Geosci.* Submitted.
- Renninger, M. (1937). *Z. Kristallogr.* **97**, 107–121.
- Ruffer, R. & Chumakov, A. I. (1996). *Hyperfine Interact.* **97/98**, 589–604.
- Seto, M., Masuda, R., Higashitaniguchi, S., Kitao, S., Kobayashi, Y., Inaba, C., Mitsui, T. & Yoda, Y. (2009). *J. Phys. Conf. Ser.* **217**, 012002.
- Smirnov, G. V. (2000). *Hyperfine Interact.* **125**, 91–112.
- Smirnov, G. V., Chumakov, A. I., Potapkin, V., Ruffer, R. & Popov, S. L. (2011). *Phys. Rev. A*, **84**, 053851.
- Smirnov, G. V., Sklyarevskii, V. V., Voscanian, R. A. & Artem'ev, A. N. (1969). *JETP Lett.* **9**, 70–73.
- Smirnov, G. V., van Bürck, U., Chumakov, A. I., Baron, A. Q. R. & Ruffer, R. (1997). *Phys. Rev. B*, **55**, 5811–5815.
- Smirnov, G. V., Zelepukhin, M. V. & van Bürck, U. (1986). *JETP Lett.* **43**, 352–355.
- Stankov, S., Ruffer, R., Sladeczek, M., Rennhofer, M., Sepiol, B., Vogl, G., Spiridis, N., Slezak, T. & Korecki, J. (2008). *Rev. Sci. Instrum.* **79**, 045108.
- Yoshida, Y., Suzuki, K., Hayakawa, K., Yukihiro, K. & Soejima, H. (2009). *Hyperfine Interact.* **188**, 121–126.
- Zelepukhin, M. V., Smirnov, G. V. & van Bürck, U. (1985). *Vopr. At. Nauk. Tekh.* **4**, 76–77. (In Russian.)